Higher-Order Band Topology in Twisted Moiré Superlattice

Bing Liu,[1] Lede Xian,[2] Haimen Mu,[1] Gan Zhao,[1] Zhao Liu,[1] Angel Rubio,[2,3,4] and Z. F. Wang[1,*]

[1]*Hefei National Laboratory for Physical Sciences at the Microscale, CAS Key Laboratory of Strongly-Coupled Quantum Matter Physics, Department of Physics, University of Science and Technology of China, Hefei, Anhui 230026, China*

[2]*Max Planck Institute for the Structure and Dynamics of Matter, Center for Free Electron Laser Science, Luruper Chaussee 149, 22761 Hamburg, Germany*

[3]*Center for Computational Quantum Physics, Simons Foundation Flatiron Institute, New York, New York 10010, USA*

[4]*Nano-Bio Spectroscopy Group, Departamento de Fisica de Materiales, Universidad del País Vasco, UPV/EHU-20018 San Sebastián, Spain*

(Received 11 August 2020; accepted 21 January 2021; published 12 February 2021)

The two-dimensional (2D) twisted bilayer materials with van der Waals coupling have ignited great research interests, paving a new way to explore the emergent quantum phenomena by twist degree of freedom. Generally, with the decreasing of twist angle, the enhanced interlayer coupling will gradually flatten the low-energy bands and isolate them by two high-energy gaps at zero and full filling, respectively. Although the correlation and topological physics in the low-energy flat bands have been intensively studied, little information is available for these two emerging gaps. In this Letter, we predict a 2D second-order topological insulator (SOTI) for twisted bilayer graphene and twisted bilayer boron nitride in both zero and full filling gaps. Employing a tight-binding Hamiltonian based on first-principles calculations, three unique fingerprints of 2D SOTI are identified, that is, nonzero bulk topological index, gapped topological edge state, and in-gap topological corner state. Most remarkably, the 2D SOTI exists in a wide range of commensurate twist angles, which is robust to microscopic structure disorder and twist center, greatly facilitating the possible experimental measurement. Our results not only extend the higher-order band topology to massless and massive twisted moiré superlattice, but also demonstrate the importance of high-energy bands for fully understanding the nontrivial electronics.

DOI: 10.1103/PhysRevLett.126.066401

Since the discovery of graphene, the two-dimensional (2D) materials have lead the fundamental research in the field of condensed-matter physics and material science. Recently, the twist degree of freedom has opened up a new avenue to manipulate the van der Waals coupled 2D materials [1]. When two layers are rotated with respect to each other, a complex moiré superlattice is formed. The interlayer coupling plays a significant role for modifying the band structure of moiré superlattice [2–9], and a variety of new physics have been discovered in this extraordinary system. One prototypical example is the twisted bilayer graphene (TBG), from the renormalized Fermi velocity and van Hove singularity associated with single-body physics [10–12], to the correlated insulator and unconventional superconductivity associated with many-body physics [13–17]. Besides the correlation effect, another interesting discovery in TBG is the nontrivial band topology in the low-energy flat bands near magic angles [18]. The relevant quantum valley Hall [19] and quantum anomalous Hall [20] in TBG were reported experimentally. Moreover, the flat band physics has also been extended to the twisted bilayer boron nitride (TBBN) [21,22] and twisted transition metal dichalcogenide [23,24], showing the similarity between massless and massive twisted moiré superlattice. However, all these prior works mainly focus on the low-energy bands of the twisted moiré superlattice, greatly neglecting the contribution of the other high-energy bands.

Higher-order topological insulator (HOTI) represents a special class of topological material. Beyond the conventional bulk-boundary correspondence, the bulk topology of an m-dimensional nth-order TI is manifested as gapless state at $(m\text{-}n)$-dimensional boundary, and gapped state otherwise [25,26]. Different to time-reversal symmetry protected TI, HOTI is protected by crystalline symmetry or chiral symmetry [27,28]. The spin-orbital coupling (SOC) is not a necessary requirement in HOTI, making it possible to study SOC-free band topology [29]. Although HOTIs have been intensively studied in theoretical models [30–33], it still remains a challenging task to realize them in real materials. Three-dimensional second-order topological insulator (3D SOTI) was reported in SnTe [34], Bi [35], $EuIn_2As_2$ [36], and $MoTe_2$ [37]. While 2D SOTI was experimentally confirmed in many artificial systems [38–43], but seldom in real materials. Recently, graphdiyne [44,45], γ graphyne [46], and TBG [47] were predicted to be carbon-based 2D SOTI in their low-energy gaps.

The nontrivial gap in graphdiyne and γ graphyne is very large (0.5 eV and 0.9 eV). However, the intervalley scattering induced nontrivial Dirac gap in TBG is extremely small (9 meV), greatly hindering the possible detection of in-gap topological corner states within current experimental resolution.

In this Letter, beyond the low-energy Dirac bands, we predict a 2D SOTI in two sizable high-energy gaps of TBG and TBBN at both zero and full fillings. Based on tight-binding (TB) model, the bulk topological index, gapped topological edge state and in-gap topological corner state are calculated to identify the higher-order band topology. Moreover, the robustness of 2D SOTI against microscopic configuration is confirmed by including local structure disorder and changing twist center. Since the nontrivial gap of TBG (0.9° to 2.5°, the largest gap goes up to 60 meV) and TBBN (0.8° to 5.1°, the largest gap goes up to 102 meV) exist in a wide range of commensurate twist angles, we believe our proposal has a strong feasibility to be detected by transport and scanning tunneling microscopy (STM) measurement, which may draw immediate experimental attention.

The characterized bands for massless and massive twisted moiré superlattice without interlayer coupling are shown schematically in Figs. 1(a) and 1(b), respectively. Turning on the interlayer coupling, one notices that the band degeneracies between different layers are lifted, and two symmetric high-energy gaps (Δ_{up} and Δ_{low}, corresponding to full and zero filling of the low-energy bands in transport measurement) appear above and below the Fermi level, as shown schematically in Figs. 1(c) and 1(d). Depending on the twist angle, these two emerging gaps can be either local or global. Interestingly, we found a higher-order band topology in both of them, that is a 2D SOTI. In the following part, the massless TBG and massive TBBN are used as two typical examples to identify this discovery in twisted moiré superlattice.

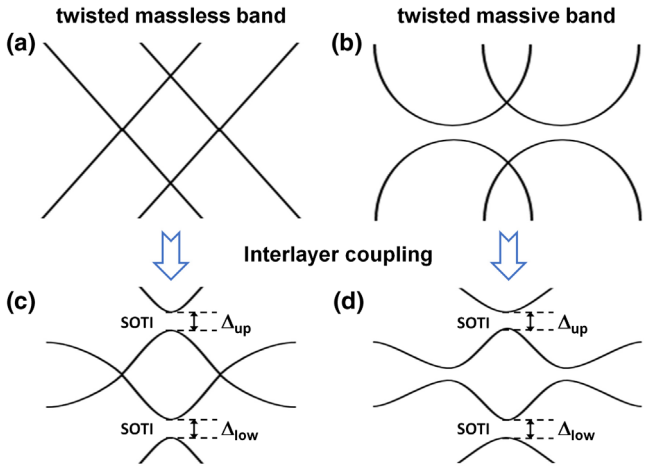

FIG. 1. Higher-order band topology in twisted moiré superlattice. (a) and (b) Schematic twisted massless and massive bands without interlayer coupling. (c) and (d) are the same as (a) and (b), but with interlayer coupling. The interlayer coupling induced two high-energy gaps are labeled as Δ_{up} and Δ_{low}, sustaining the 2D SOTI.

The atomic structure of TBG is constructed by rotating one layer in an *AA*-stacking bilayer graphene with a twist center at hexagon-ring center (belonging to point group D_6), as shown in Fig. 2(a). Figure 2(b) shows the first Brillouin (BZ) of TBG and its projected edge BZ, where the high-symmetric k points are labeled. The typical band structures of TBG with different commensurate twist angles are shown in Figs. 2(c)–2(h). With the decreasing of twist angle from 5.1° to 1.1°, two significant characters can be found. First, the low-energy bands are gradually isolated from the other high-energy bands by one upper and one lower gap (Δ_{up} and Δ_{low}), as highlighted by the blue- and red-color region, respectively. Second, the dispersion of low-energy bands is gradually reduced, tuning the band shape from Dirac to flat. These noticeable results are consistent with previous theoretical work [48]. Furthermore, the gap size of Δ_{up} and Δ_{low} vs twist angle θ is shown in Figs. 2(i) and 2(j), respectively. One can see that the global gap exists in a wide range of θ, from 0.9° to 2.5°, showing a nonmonotonic behavior and approaching the maximum value of 60 meV at 1.2°. Recently, similar gap size variation in TBG was also observed in STM experiment [49], further demonstrating the reliability of our TB results.

To identify the bulk topology of TBG in these two high-energy gaps, its fractional corner charge (Q) is checked, which is a bulk topological index for classifying the higher-order band topology [50]. In a 2D system with C_{6z} and T

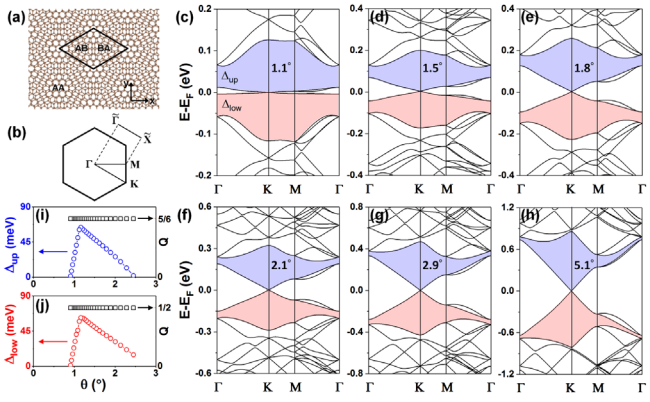

FIG. 2. Bulk topology of TBG with different commensurate twist angles. (a) Atomic structure of TBG with a large twist angle. The black line denotes the unit cell, and the labels *AA*, *AB*, and *BA* denote different stacking regions. (b) First BZ of TBG and projected edge BZ with high-symmetric k points. (c)–(h) Band structures of TBG with different commensurate twist angles. The blue- and red-color region denotes the upper and lower gap for isolating the low-energy bands from other high-energy bands, labeled as Δ_{up} and Δ_{low}, respectively. (i) Δ_{up} and its topological index Q vs the twist angle θ. (j) is the same as (i), but for Δ_{low}.

symmetries, it can be directly evaluated as [50] $Q = [M_1^{(2)}]/4 + [K_1^{(3)}]/6 \bmod 1$, where $[M_1^{(2)}]$ ($[K_1^{(3)}]$) denotes the band number difference below the energy gap for C_{2z} (C_{3z}) symmetry with eigenvalue 1 between M (K) and Γ point. The nonzero Q in the upper and lower gap is shown in Figs. 2(i) and 2(j), respectively, indicating TBG to be a 2D SOTI. Physically, this nontrivial bulk topology can also be understood from an intuitive picture, called the double band inversion [51,57].

Moreover, due to the modified bulk-boundary correspondence, 2D SOTI is characterized by gapped topological edge state and in-gap topological corner state [44–47], which can be used as a fingerprint to distinguish it from other topological phases. Since the nontrivial bulk topology of TBG is the same for twist angle within 0.9°–2.5°, in order to simplify our calculations, we will focus on $\theta = 2.1°$ to illustrate its edge and corner states (similar results are obtained for $\theta = 1.8°$, see Fig. S1 [51]). To identify the edge topology of TBG, based on recursive Green's function method [58,59], the semi-infinite spectral function along the edge cutting through AA-stacking region is calculated in both upper and lower gap, as shown in Figs. 3(a) and 3(b), respectively. Obviously, there is one pair of gapped topological edge states within the energy window of both gaps, confirming the first unique boundary character. In the upper gap [Fig. 3(a)], the top branch of topological edge state gradually merges into the bulk states at higher energy, while the bottom branch of topological edge state always detaches from the bulk states, forming a gap between them at the Γ point. In the lower gap [Fig. 3(b)], the gap between the top and bottom branch of the topological edge state is still at the Γ point, but the band shape is opposite to the former case. In principle, this band shape can be attributed to the approximate electron-hole symmetry in TBG, making the bulk and edge states almost symmetric with respect to the Fermi level.

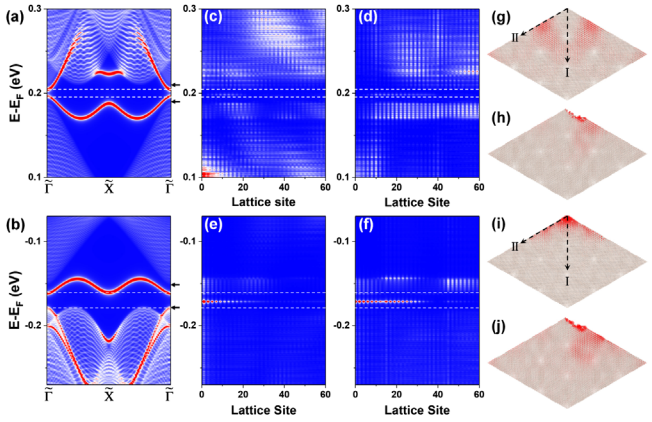

FIG. 3. Edge and corner topology of TBG for $\theta = 2.1°$. (a) and (b) Semi-infinite spectral function of TBG along the edge in the upper and lower gap, showing the gapped topological edge states. The black arrows denote the corresponding bulk gap edges. (c) and (d) Line-scanning LDOS along the dashed-arrow direction in the upper gap, labeled as I and II around the corner in (g), showing the energy level of in-gap topological corner state. (e) and (f) are the same as (c) and (d), but in the lower gap. (g) and (i) Spatial distribution of in-gap topological corner states around the 120° corner in the upper and lower gap. The circle size denotes the weighting factor of corner states. (h) and (j) are the same as (g) and (i), but including structure disorder at the corner. The structure in (g) to (j) is the corner part of the whole TBG cluster, where only the top region is a real corner.

To identify the corner topology of TBG, based on the Lanczos recursive method [6], the local density of states (LDOS) around a 120° corner with two edges cutting through the AA-stacking region is calculated in both upper and lower gaps. To avoid the finite-size effect, a huge rhombus TBG cluster is constructed by extending the unit cell of TBG to a 20×20 supercell with over 1×10^6 atoms. Around the corner, a line scanning along two dashed-arrow directions [labeled as I and II in Figs. 3(g) and 3(i)] is calculated. In the upper gap, the energy and position dependent LDOS along lines I and II is shown in Figs. 3(c) and 3(d), respectively. Aligning them with the spectral function in Fig. 3(a), three significant features can be observed: (1) there is one state within the energy window of gapped topological edge states (two dashed yellow lines are used to guide eyes); (2) the energy level of this state is the same along both lines I and II; (3) the intensity of this state decays quickly away from the corner. Combing all these features, it is clear that the observed in-gap state is a topological corner state in TBG. To further illustrate its spatial distribution, the LDOS around the corner in a 3×3 region is plotted at this energy level. The localized topological corner state is shown in Fig. 3(g), confirming the second unique boundary character of 2D SOTI. In the lower gap, the similar line-scanning results are observable, but the in-gap state has a stronger intensity, as shown in Figs. 3(e) and 3(f). The spatial distribution of this in-gap topological corner state is shown in Fig. 3(i), which is more localized than that in the upper gap. Here, the different spatial distribution of the corner states in Figs. 3(g) and 3(i) can be attributed to the symmetry related corner charge difference between the upper and lower gap, which is $Q = 5/6$ and $1/2$, respectively. Therefore, from bulk, edge, and corner three aspects, we have directly confirmed the 2D SOTI in TBG.

Physically, the topological corner state of TBG can be understood in an alternative way. Starting from a pair of gapped topological edge states on one edge of TBG, the effective Hamiltonian is described by [51,60] $H = k\sigma_z + m\sigma_x$, where k is the momentum along the edge, m is the mass term, and σ is the Pauli matrix in the edge-state space. At the 120° corner of TBG, one notices that its two edges are connected with $C_{2y} = \sigma_y$ symmetry. Since $C_{2y}(m\sigma_x)C_{2y}^{-1} = -m\sigma_x$, that is, m is odd between these two edges and the mass term will be inverted crossing the 120° corner. Therefore, the observed topological corner state in

TBG is equivalent to the domain wall state between two gapped edge states with opposite mass (see Fig. S2 [51]). Similarly, this mechanism can also explain why there is no topological corner state at the 60° corner of TBG, where two edges are connected with $C_{2x} = \sigma_x$ symmetry. Because m is even under C_{2x}, the mass term is not inverted crossing the 60° corner.

To facilitate the possible experimental measurement, the robustness of topological corner state in TBG against the microscopic structural disorder and twist center is also investigated. The structural disorder is simulated by removing carbon atoms randomly around the corner, then, the LDOS is recalculated at the same energy level to characterize the in-gap topological corner state. As shown in Figs. 3(h) and 3(j), the topological corner state in the upper and lower gap is very robust, which is still localized at corner region but with a different spatial distribution. Moreover, starting from an *AA*-stacking bilayer graphene, another frequently studied TBG is constructed by choosing twist center at single-atom (belonging to point group D_3). Using this new configuration, similar gapped topological edge states and in-gap topological corner states are found in both upper and lower gaps (see Fig. S3 [51]). Consequently, the 2D SOTI in TBG is robust to finite microscopic perturbations, further demonstrating the topological origin of these in-gap corner states.

Although 2D SOTI in TBG has been studied in previous Park's work [47], one notices that the nontrivial gap opening mechanism and the symmetry requirement for realizing this higher-order topological state are dramatically different to our proposal. Most remarkably, our proposed 2D SOTI not only exists in massless TBG, but also exists in massive TBBN, which can be described by the same theoretical framework. The TBBN is constructed by rotating one layer in an *AA*-stacking bilayer BN with a twist center at hexagon-ring center (belonging to point group D_3). The typical band structure of TBBN for $\theta = 3.9°$ is shown in Fig. 4(a) (see Fig. S4 for more twist angles [51]). Except the insulating gap at Fermi level, the low-energy band feature is comparable to that in TBG. Obviously, two global high-energy gaps exist in a wide range of commensurate twist angle from 0.8° to 5.1°, as shown in Figs. 4(b) and 4(c). The largest gap size goes up to 102 meV at 3.1°, almost twice the value in TBG. Since TBBN has C_{3z} and T symmetries, its bulk topological index can be evaluated as [50] $Q = [K_2^{(3)}]/3 \bmod 1$, where $[K_2^{(3)}]$ denotes the band number difference below the energy gap for C_{3z} symmetry with eigenvalue $\exp(i2\pi/3)$ between the K and Γ point. The nonzero Q in the upper and lower gap is shown in Figs. 4(b) and 4(c), respectively, demonstrating the same nontrivial bulk topology from 0.8° to 5.1°. Furthermore, focusing on $\theta = 3.9°$ with the edge cutting through *AA*-stacking region, the gapped topological edge state and in-gap topological corner state in the upper (lower) gap of TBBN is shown in Figs. 4(d) [Fig. 4(e)] and 4(f) [Fig. 4(g)], respectively, which is comparable to those in TBG. Therefore, the TBBN is also confirmed to be a 2D SOTI.

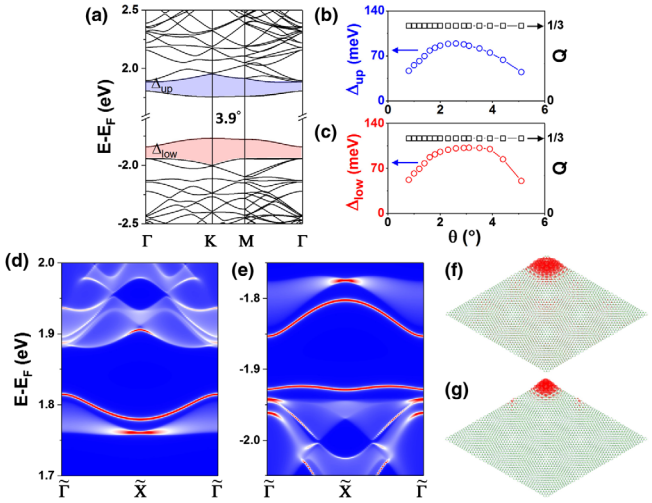

FIG. 4. 2D SOTI in TBBN. (a) Band structure of TBBN for $\theta = 3.9°$. (b) Δ_{up} and its topological index Q vs the twist angle θ. (c) is the same as (b), but for Δ_{low}. (d) and (e) Semi-infinite spectral function of TBBN along the edge in the upper and lower gap. (f) and (g) Spatial distribution of in-gap topological corner states around the 120° corner in the upper and lower gap. The structure in (f) and (g) is the corner part of the whole TBBN cluster, where only the top region is a real corner.

The Fermi level of TBG and TBBN is not in the nontrivial high-energy gaps, thus doping is needed to detect the edge and corner states. This requires doping four electrons or holes per unit cell, corresponding to a doping concentration of $1.9 \times 10^{12} \sim 1.4 \times 10^{13}$ cm^{-2} for $\theta = 0.9°$–$2.5°$ in TBG and $1.6 \times 10^{12} \sim 5.8 \times 10^{13}$ cm^{-2} for $\theta = 0.8°$–$5.1°$ in TBBN. Experimentally, this is achievable by electrostatic gating, and the doping concentration in graphene can be up to 4×10^{14} cm^{-2} for both electron and hole by using a solid polymer electrolyte gate [61]. Recently, the topological corner state relevant transport properties have also been studied. Park *et al.* proposed an instanton tunneling oscillation between the corner states in the low-energy Dirac gap of TBG [62], showing a unique feature to distinguish the trivial and nontrivial corner states. Ma *et al.* reported a nonlocal transport measurement, and found some nonquantized signals in two high-energy gaps of TBG [63], which are attributed to the corner state channels by bulk topological index calculation alone. Since our results provide direct theoretical evidence to show the existence of topological corner states in both TBG and TBBN, these interesting physical effects for the corner states are expected for both massless and massive moiré superlattice, which can be detected by transport and STM measurement, deserving to be further investigated.

In summary, we demonstrate the existence of a stable 2D SOTI in both zero and full filling gaps of TBG and TBBN,

which is identified through bulk topological index, gapped topological edge state, and in-gap topological corner calculations. Our results enrich the topological physics in massless and massive twisted moiré superlattice, and greatly extend the candidate realistic materials of 2D SOTI. These new discoveries may draw more fundamental research interests and provide a chance to explore the correlation between higher-order band topology and superconductivity in the future.

This work was supported by the National Natural Science Foundation of China (Grants No. 11774325 and No. 21603210), National Key Research and Development Program of China (Grant No. 2017YFA0204904), Fundamental Research Funds for the Central Universities. L. X. and A. R. were supported by the European Research Council (ERC-2015-AdG-694097), Grupos Consolidados (IT1249-19), the Cluster of Excellence "Advanced Imaging of Matter" (AIM) and SFB925 "Light induced dynamics and control of correlated quantum systems." The Flatiron Institute is a division of the Simons Foundation. We thank Supercomputing Center at USTC for providing the computing resources.

*zfwang15@ustc.edu.cn

[1] S. Carr, S. Fang, and E. Kaxiras, Nat. Rev. Mater. **5**, 748 (2020).
[2] J. M. B. Lopes dos Santos, N. M. R. Peres, and A. H. Castro Neto, Phys. Rev. Lett. **99**, 256802 (2007).
[3] G. Trambly de Laissardière, D. Mayou, and L. Magaud, Nano Lett. **10**, 804 (2010).
[4] E. Suárez Morell, J. D. Correa, P. Vargas, M. Pacheco, and Z. Barticevic, Phys. Rev. B **82**, 121407(R) (2010).
[5] R. Bistritzer and A. H. MacDonald, Proc. Natl. Acad. Sci. U.S.A. **108**, 12233 (2011).
[6] Z. F. Wang, F. Liu, and M. Y. Chou, Nano Lett. **12**, 3833 (2012).
[7] S. Javvaji, J.-H. Sun, and J. Jung, Phys. Rev. B **101**, 125411 (2020).
[8] T. Salamon, A. Celi, R. W. Chhajlany, I. Frérot, M. Lewenstein, L. Tarruell, and D. Rakshit, Phys. Rev. Lett. **125**, 030504 (2020).
[9] T. Salamon, R. W. Chhajlany, A. Dauphin, M. Lewenstein, and D. Rakshit, Phys. Rev. B **102**, 235126 (2020).
[10] G. Li, A. Luican, J. M. B. Lopes dos Santos, A. H. Castro Neto, A. Reina, J. Kong, and E. Y. Andrei, Nat. Phys. **6**, 109 (2010).
[11] A. Luican, Guohong Li, A. Reina, J. Kong, R. R. Nair, K. S. Novoselov, A. K. Geim, and E. Y. Andrei, Phys. Rev. Lett. **106**, 126802 (2011).
[12] I. Brihuega, P. Mallet, H. González-Herrero, G. Trambly de Laissardière, M. M. Ugeda, L. Magaud, J. M. Gómez-Rodríguez, F. Ynduráin, and J.-Y. Veuillen, Phys. Rev. Lett. **109**, 196802 (2012).
[13] Y. Cao, V. Fatemi, A. Demir, S. Fang, S. L. Tomarken, J. Y. Luo, J. D. Sanchez-Yamagishi, K. Watanabe, T. Taniguchi, E. Kaxiras, R. C. Ashoori, and P. Jarillo-Herrero, Nature (London) **556**, 80 (2018).
[14] Y. Cao, V. Fatemi, S. Fang, K. Watanabe, T. Taniguchi, E. Kaxiras, and P. Jarillo-Herrero, Nature (London) **556**, 43 (2018).
[15] M. Yankowitz, S. Chen, H. Polshyn, Y. Zhang, K. Watanabe, T. Taniguchi, D. Graf, A. F. Young, and C. R. Dean, Science **363**, 1059 (2019).
[16] A. Kerelsky, L. J. McGilly, D. M. Kennes, L. Xian, M. Yankowitz, S. Chen, K. Watanabe, T. Taniguchi, J. Hone, C. Dean, A. Rubio, and A. N. Pasupathy, Nature (London) **572**, 95 (2019).
[17] Y. Xie, B. Lian, B. Jäck, X. Liu, C.-L. Chiu, K. Watanabe, T. Taniguchi, B. A. Bernevig, and A. Yazdani, Nature (London) **572**, 101 (2019).
[18] Z. Song, Z. Wang, W. Shi, G. Li, C. Fang, and B. A. Bernevig, Phys. Rev. Lett. **123**, 036401 (2019).
[19] P. Rickhaus, J. Wallbank, S. Slizovskiy, R. Pisoni, H. Overweg, Y. Lee, M. Eich, M.-H. Liu, K. Watanabe, T. Taniguchi, T. Ihn, and K. Ensslin, Nano Lett. **18**, 6725 (2018).
[20] M. Serlin, C. L. Tschirhart, H. Polshyn, Y. Zhang, J. Zhu, K. Watanabe, T. Taniguchi, L. Balents, and A. F. Young, Science **367**, 900 (2020).
[21] L. Xian, D. M. Kennes, N. Tancogne-Dejean, M. Altarelli, and A. Rubio, Nano Lett. **19**, 4934 (2019).
[22] X. J. Zhao, Y. Yang, D. B. Zhang, and S. H. Wei, Phys. Rev. Lett. **124**, 086401 (2020).
[23] F. Wu, T. Lovorn, E. Tutuc, I. Martin, and A. H. MacDonald, Phys. Rev. Lett. **122**, 086402 (2019).
[24] L. Wang, E.-M. Shih, A. Ghiotto, L. Xian, D. A. Rhodes, C. Tan, M. Claassen, D. M. Kennes, Y. Bai, B. Kim, K. Watanabe, T. Taniguchi, X. Zhu, J. Hone, A. Rubio, A. N. Pasupathy, and C. R. Dean, Nat. Mater. **19**, 861 (2020).
[25] W. A. Benalcazar, B. A. Bernevig, and T. L. Hughes, Phys. Rev. B **96**, 245115 (2017).
[26] W. A. Benalcazar, B. A. Bernevig, and T. L. Hughes, Science **357**, 61 (2017).
[27] Z. Song, Z. Fang, and C. Fang, Phys. Rev. Lett. **119**, 246402 (2017).
[28] R. Okugawa, S. Hayashi, and T. Nakanishi, Phys. Rev. B **100**, 235302 (2019).
[29] A. Alexandradinata, C. Fang, M. J. Gilbert, and B. A. Bernevig, Phys. Rev. Lett. **113**, 116403 (2014).
[30] M. Ezawa, Phys. Rev. Lett. **120**, 026801 (2018).
[31] R.-X. Zhang, W. S. Cole, X. Wu, and S. Das Sarma, Phys. Rev. Lett. **123**, 167001 (2019).
[32] R. Chen, C.-Z. Chen, J.-H. Gao, B. Zhou, and D.-H. Xu, Phys. Rev. Lett. **124**, 036803 (2020).
[33] H. Li and K. Sun, Phys. Rev. Lett. **124**, 036401 (2020).
[34] F. Schindler, A. M. Cook, M. G. Vergniory, Z. Wang, S. S. P. Parkin, B. A. Bernevig, and T. Neupert, Sci. Adv. **4**, eaat0346 (2018).
[35] F. Schindler, Z. Wang, M. G. Vergniory, A. M. Cook, A. Murani, S. Sengupta, A. Yu. Kasumov, R. Deblock, S. Jeon, I. Drozdov, H. Bouchiat, S. Guéron, A. Yazdani, B. A. Bernevig, and T. Neupert, Nat. Phys. **14**, 918 (2018).
[36] Y. Xu, Z. Song, Z. Wang, H. Weng, and X. Dai, Phys. Rev. Lett. **122**, 256402 (2019).

[37] Z. Wang, B. J. Wieder, J. Li, B. Yan, and B. A. Bernevig, Phys. Rev. Lett. **123**, 186401 (2019).
[38] M. Serra-Garcia1, V. Peri, R. Süsstrunk, O. R. Bilal, T. Larsen, L. G. Villanueva, and S. D. Huber, Nature (London) **555**, 342 (2018).
[39] C. W. Peterson, W. A. Benalcazar, T. L. Hughes, and G. Bahl, Nature (London) **555**, 346 (2018).
[40] S. Imhof, C. Berger, F. Bayer, J. Brehm, L. W. Molenkamp, T. Kiessling, F. Schindler, C. H. Lee, M. Greiter, T. Neupert, and R. Thomale, Nat. Phys. **14**, 925 (2018).
[41] H. Xue, Y. Yang, F. Gao, Y. Chong, and B. Zhang, Nat. Mater. **18**, 108 (2019).
[42] X. Ni, M. Weiner, A. Alù, and A. B. Khanikaev, Nat. Mater. **18**, 113 (2019).
[43] J. Noh, W. A. Benalcazar, S. Huang, M. J. Collins, K. P. Chen, T. L. Hughes, and M. C. Rechtsman, Nat. Photonics **12**, 408 (2018).
[44] E. Lee, R. Kim, J. Ahn, and B.-J. Yang, npj Quantum Mater. **5**, 1 (2020).
[45] X.-L. Sheng, C. Chen, H. Liu, Z. Chen, Z.-M. Yu, Y. X. Zhao, and S. A. Yang, Phys. Rev. Lett. **123**, 256402 (2019).
[46] B. Liu, G. Zhao, Z. Liu, and Z. F. Wang, Nano Lett. **19**, 6492 (2019).
[47] M. J. Park, Y. Kim, G. Y. Cho, and S. B. Lee, Phys. Rev. Lett. **123**, 216803 (2019).
[48] S. Carr, S. Fang, Z. Zhu, and E. Kaxiras, Phys. Rev. Research **1**, 013001 (2019).
[49] Y. Choi, J. Kemmer, Y. Peng, A. Thomson, H. Arora, R. Polski, Y. Zhang, H. Ren, J. Alicea, G. Refael, F. von Oppen, K. Watanabe, T. Taniguchi, and S. Nadj-Perge, Nat. Phys. **15**, 1174 (2019).
[50] W. A. Benalcazar, T. Li, and T. L. Hughes, Phys. Rev. B **99**, 245151 (2019).
[51] See Supplemental Material at http://link.aps.org/supplemental/10.1103/PhysRevLett.126.066401 for calculation methods and additional tight-binding and first-principles results, which includes Refs. [52–56].
[52] P. Moon and M. Koshino, Phys. Rev. B **87**, 205404 (2013).
[53] S. Plimpton, J. Comput. Phys. **117**, 1 (1995).
[54] G. Kresse and J. Furthmüller, Phys. Rev. B **54**, 11169 (1996).
[55] A. Alexandradinata, X. Dai, and B. A. Bernevig, Phys. Rev. B **89**, 155114 (2014).
[56] M. Kindermann, Phys. Rev. Lett. **114**, 226802 (2015).
[57] C.-H. Hsu, X. Zhou, T.-R. Chang, Q. Ma, N. Gedik, A. Bansil, S.-Y. Xu, H. Lin, and L. Fu, Proc. Natl. Acad. Sci. U.S.A. **116**, 13255 (2019).
[58] M. P. Lopez Sancho, J. M. Lopez Sancho, J. M. L. Sancho, and J. Rubio, J. Phys. F **15**, 851 (1985).
[59] Z. Liu, Y. Jin, Y. Yang, Z. F. Wang, and J. Yang, New J. Phys. **20**, 023041 (2018).
[60] Y.-Q. Wang and J. E. Moore, Phys. Rev. B **99**, 155102 (2019).
[61] D. K. Efetov and P. Kim, Phys. Rev. Lett. **105**, 256805 (2010).
[62] M. J. Park, S. Jeon, S. Lee, H. C. Park, and Y. Kim, Carbon **174**, 260 (2021).
[63] C. Ma, Q. Wang, S. Mills, X. Chen, B. Deng, S. Yuan, C. Li, K. Watanabe, T. Taniguchi, X. Du, F. Zhang, and F. Xia, Nano Lett. **20**, 6076 (2020).